Proceedings of ASME Turbo Expo 2011
GT2011
June 6-10, 2011, Vancouver, British Columbia, Canada

GT2011-45721

INFLUENCE OF FILM COOLING HOLE ANGLES AND GEOMETRIES ON AERODYNAMIC LOSS AND NET HEAT FLUX REDUCTION

Chia Hui Lim, Graham Pullan
Whittle Laboratory
University of Cambridge
Cambridge, CB3 0DY, UK
Email: chl44@cam.ac.uk, gp10006@cam.ac.uk

Peter Ireland
Rolls-Royce plc
PO Box 31
Derby, UK
Email: peter.ireland@rolls-royce.com

ABSTRACT

Turbine design engineers have to ensure that film cooling can provide sufficient protection to turbine blades from the hot mainstream gas, while keeping the losses low. Film cooling hole design parameters include inclination angle (α), compound angle (β), hole inlet geometry and hole exit geometry. The influence of these parameters on aerodynamic loss and net heat flux reduction is investigated, with loss being the primary focus. Low-speed flat plate experiments have been conducted at momentum flux ratios of $IR = 0.16$, 0.64 and 1.44.

The film cooling aerodynamic mixing loss, generated by the mixing of mainstream and coolant, can be quantified using a three-dimensional analytical model that has been previously reported by the authors. The model suggests that for the same flow conditions, the aerodynamic mixing loss is the same for holes with different α and β but with the same angle between the mainstream and coolant flow directions (angle κ). This relationship is assessed through experiments by testing two sets of cylindrical holes with different α and β: one set with $\kappa = 35°$, another set with $\kappa = 60°$. The data confirm the stated relationship between α, β, κ and the aerodynamic mixing loss. The results show that the designer should minimise κ to obtain the lowest loss, but maximise β to achieve the best heat transfer performance. A suggestion on improving the loss model is also given.

Five different hole geometries ($\alpha = 35.0°$, $\beta = 0°$) were also tested: cylindrical hole, trenched hole, fan-shaped hole, D-Fan and SD-Fan. The D-Fan and the SD-Fan have similar hole exits to the fan-shaped hole but their hole inlets are laterally expanded. The external mixing loss and the loss generated inside the hole are compared. It was found that the D-Fan and the SD-Fan have the lowest loss. This is attributed to their laterally expanded hole inlets, which lead to significant reduction in the loss generated inside the holes. As a result, the loss of these geometries is ≈ 50 % of the loss of the fan-shaped hole at $IR = 0.64$ and 1.44.

NOMENCLATURE

BR blowing ratio = $\frac{\rho_c V_c}{\rho_g V_g}$
c_p specific heat capacity at constant pressure
C_{p0} stagnation pressure coefficient
D diameter
DR density ratio = $\frac{\rho_c}{\rho_g}$
e lateral expansion angle of hole
h_f heat transfer coefficient in the presence of film cooling
h_{nfc} heat transfer coefficient with no film cooling
IR momentum flux ratio = $\frac{\rho_c V_c^2}{\rho_g V_g^2}$
L hole length
m mass flowrate
M Mach number
$NHFR$ Net Heat Flux Reduction
p pressure
P hole pitch
R gas constant
s specific entropy
V velocity
VR velocity ratio = $\frac{V_c}{V_g}$
x, y, z coordinates

α inclination angle
β compound angle
$\Delta\Sigma$ rate of entropy creation due to irreversibility
η adiabatic film cooling effectiveness
γ ratio of specific heat capacities
κ absolute angle between local mainstream and coolant flow vectors
ϕ mass flowrate ratio of coolant to mainstream = m_c/m_g
ρ density
θ non-dimensional temperature
φ angle between hole axis and plane tangent to the point on the blade surface where the coolant is ejected
ξ_x streamwise vorticity
ζ entropy loss coefficient
ζ_{hole} entropy loss coefficient for aerodynamic loss generated inside the hole
ζ_{mix} entropy loss coefficient for aerodynamic mixing loss
ζ_{total} entropy loss coefficient (total), $\zeta_{total} = \zeta_{mix} + \zeta_{hole}$

Subscripts
BL boundary layer
c coolant
g 'local mainstream' or 'mainstream conditions measured at a distance upstream of the coolant ejection'
m mixed-out flow
m,BL mixed-out flow obtained from boundary layer flow (no coolant ejection)
m,cool mixed-out flow obtained when there is coolant ejection
mix mixing
mix,KE aerodynamic mixing
mix,Q thermal mixing
w wall
0 stagnation (total)
1g mainstream conditions measured at the rig inlet

INTRODUCTION

Gas turbines operate at extremely high turbine entry temperatures (TETs), which can reach 1850 K [1]. For non-ideal turbomachinery, thermal efficiency increases with TET (Wilcock *et al*. [2]). The high TET which has been reached to date is beyond the melting point of the metals used in the turbine. Thus, the turbine components are cooled to ensure design life by the use of technologies such as advanced alloys, ceramic coatings and film cooling. In film cooling, air that has bypassed the combustor is ejected through discrete holes, in order to coat the blade external surface with a film of protective cooling air. This technology is used extensively on high pressure turbines.

The downside of film cooling is the associated losses and the present study focus on the aerodynamic loss. Young and Wilcock [3,4] developed a formal framework for modelling cooling losses, by splitting the losses into separate components for clarity. Each component is expressed in terms of a rate of entropy creation due to irreversibility ($\Delta\Sigma$), instead of stagnation pressure loss. The loss components associated with film cooling are film cooling mixing losses ($\Delta\Sigma_{mix}$), which arise due to the mixing of the mainstream flow and the ejected coolant. $\Delta\Sigma_{mix}$ consist of two components: $\Delta\Sigma_{mix,Q}$ and $\Delta\Sigma_{mix,KE}$. $\Delta\Sigma_{mix,Q}$ is the thermal mixing loss, which is produced through heat transfer when the static temperatures of the mainstream and the coolant equilibrate. $\Delta\Sigma_{mix,KE}$ is the aerodynamic mixing loss or viscous dissipation. It refers to the dissipation of the kinetic energy when the velocities of both gases equilibrate. $\Delta\Sigma_{mix,Q}$ is inevitable and exists whenever there is cooling. Nonetheless, there is scope to reduce $\Delta\Sigma_{mix,KE}$ and hence improve the cooled turbine efficiency.

Details of the estimation of $\Delta\Sigma_{mix}$ and the associated turbine efficiency decrement have been reported by Lim *et al.* [5] and only the main findings are repeated here. $\Delta\Sigma_{mix}$ can be estimated using the model proposed by Hartsel [6] and the entropy-based formulations of Young and Wilcock [4]. The model is a two-dimensional (2D) analytical control volume model where coolant is ejected at an inclination angle (α) to the mainstream flow direction. The mainstream and coolant are assumed to mix at constant static pressure. Several authors have found acceptable agreement between the simple Hartsel model and experimental data (Ito *et al.* [7], Day *et al.* [8]).

The cooling hole orientation on a blade is fixed by both the inclination angle (α) and the compound angle (β) which gives the ejected coolant a lateral component. The stated 2D model by Hartsel, however, is not suitable for coolant ejection through compound angles. Using a control volume analysis, Lim *et al.* [5] show that the model can be extended to be three-dimensional (3D), by simply replacing α of the 2D model with κ. κ is defined as the angle between the local mainstream and coolant flow vectors at the hole exit. The 3D model for $\Delta\Sigma_{mix,KE}$ is

$$\Delta\Sigma_{mix,KE} = \frac{m_c\gamma_g R_g M_g^2}{2}\left[\left(1-\frac{V_c}{V_g}\cos\kappa\right)^2+\left(\frac{V_c}{V_g}\sin\kappa\right)^2\right] \quad (1)$$

where subscripts g and c represent the local mainstream and the coolant; c_p, γ and R are the gas properties; m is the coolant mass flowrate; V is the velocity; and M is the Mach number. Equation (1) is known here as the '3D Hartsel' model. The coolant velocity vector (V_c) is assumed to be in the direction set by α and β. Figure 1 illustrates the definitions of α, β and κ. α is measured on the local plane PQRS (*xz*-plane) and V_c^{plane} is the component of V_c in the local plane PQRS. β gives the coolant a lateral *y*-component. With the local mainstream aligned with the *x*-direction, α and β are related to κ by

$$cos\kappa = cos\alpha\ cos\beta \quad (2)$$

There are other studies [9,10] which define the inclination angle as the angle between the hole axis and the plane tangent to the point on the blade surface where the coolant is ejected. This angle is known here as angle φ. When $\beta = 0^\circ$, $\alpha = \varphi$; when

$\beta \neq 0°$, $\alpha > \varphi$ (Fig. 2). In the present research, the inclination angle takes the definition of α.

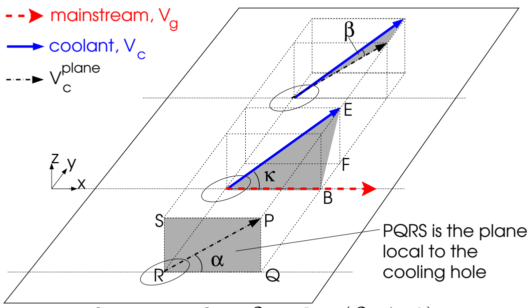

FIGURE 1: Definitions of α, β and κ ($\beta \neq 0°$) (Lim *et al.* [5])

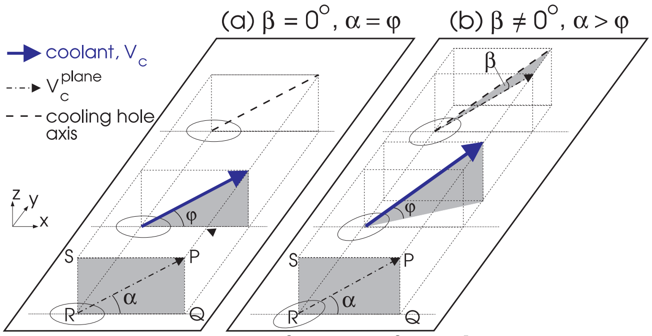

FIGURE 2: Definitions of α and φ

Equation (1) (3D Hartsel model) and Eqn. (2) are derived analytically. They suggest that for the same flow conditions, the aerodynamic mixing loss ($\Delta\Sigma_{mix,KE}$) is the same for coolant ejection through holes with different α and β but with the same κ. This relationship is assessed in this study through experiments.

The effect of β on aerodynamic loss has been investigated by Lee *et al.* [9]. They conducted experiments on a cylindrical hole with a fixed $\varphi = 30°$. The aerodynamic loss was found to increase with β. They deduced that this is due to bigger disturbance to the mainstream by the coolant jet, leading to more mixing of the mainstream and the coolant.

A review of film cooling hole geometries is given by Bunker [11]. Bunker commented that the major advancement in film cooling technology has been the use of a fan-shaped hole (the hole exit having a lateral expansion) and a laidback hole (the hole exit having a streamwise expansion into the blade surface). Goldstein *et al.* [12] was the first to report that the fan-shaped hole has a better adiabatic film cooling effectiveness than the cylindrical hole. Nevertheless, the aerodynamic loss of the fan-shaped hole is high. Annular cascade tests by Day *et al.* [8] show that the loss due to the fan-shaped hole is more than twice that of the cylindrical hole. Flat plate tests by Sargison *et al.* [13, 14] also show that the loss of the fan-shaped hole is higher than that of the cylindrical hole, for a velocity ratio of less than 1. The high loss of the fan-shaped hole is associated with the coolant separation in the lateral expansion of the hole [15] and the associated inefficient diffusion process.

Another cooling hole geometry of interest is the trenched hole, which was first reported by Bunker [16]. It consists of a streamwise cylindrical hole embedded in a shallow trench. It has better heat transfer performance than a cylindrical hole (Dorrington *et al.* [17], Harrison *et al.* [18]). The geometry is attractive because it has a lower manufacturing cost than the fan-shaped hole and the laidback hole. This is due to the fact that the shallow trench can be created using the protective Thermal Barrier Coating (TBC), without machining into the blade metal (Bunker [11]). Nonetheless, according to the authors' knowledge, there is no open literature data on the trenched hole aerodynamic loss.

The converging slot-hole or 'console' has a lower aerodynamic loss than the cylindrical hole and the fan-shaped hole (Sargison *et al.* [13, 14]). It has a circular inlet which transitions to a slot at the exit, with convergence in the streamwise direction and divergence in the lateral direction. The convergence is greater than the divergence so that the cross-sectional area decreases.

Details on the manufacturing of different film cooling hole geometries are provided by Bunker [11, 19]. Cooling holes can be drilled by the following techniques: laser, electro-discharge machining (EDM) and abrasive water jet.

Research objectives

This experimental study on film cooling has the following objectives:

1. to quantify the influence of hole angles, hole inlet geometry and hole exit geometry on film cooling aerodynamic loss
2. to assess the relationship linking α, β, κ and the aerodynamic mixing loss, as suggested by the 3D Hartsel model
3. to assess the analytical 3D Hartsel model through experiments
4. to measure the aerodynamic loss of trenched hole, drilled fan-shaped hole (D-Fan) and smooth drilled fan-shaped hole (SD-Fan)

Two groups of geometries were tested for their aerodynamic loss: (i) cylindrical holes with different α and β but with the same κ; (ii) streamwise holes with different hole inlet and hole exit geometries.

The geometries were also assessed for their heat transfer performance. However, a detailed report of the heat transfer study is beyond the scope of this paper.

This paper is divided into three sections. First, the experimental setup and method for both the aerodynamic loss and the heat transfer measurements are described; this includes details of the hole geometries. Next, the aerodynamic loss and heat transfer results for the first group of geometries (cylindrical holes) are presented, followed by the results for the second group.

EXPERIMENTAL SETUP AND METHOD

Experimental rig design

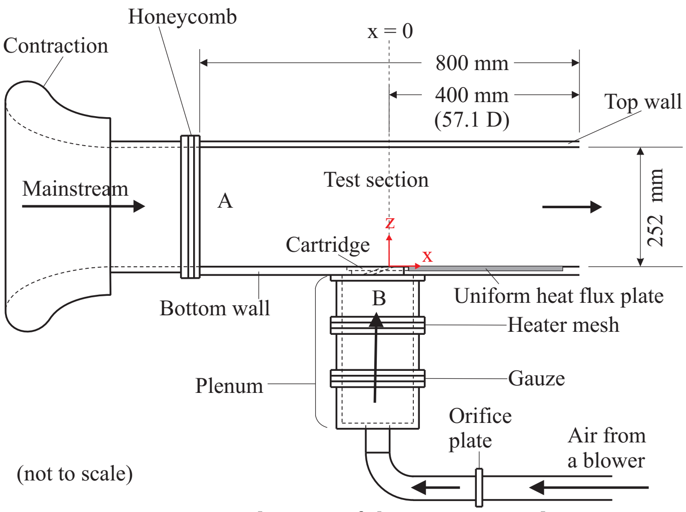

FIGURE 3: Side view of the experimental rig

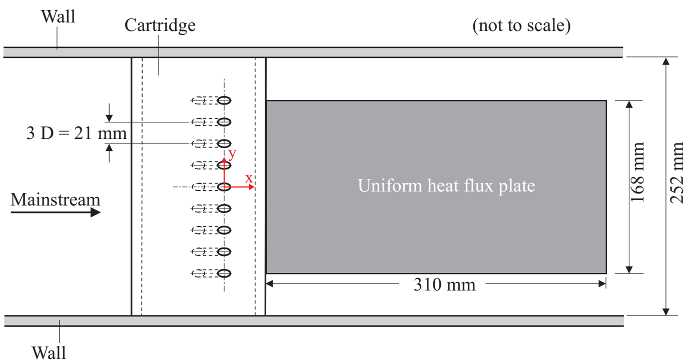

FIGURE 4: Plan view of the test section flat plate

Figure 3 presents the side view of the low-speed flat plate rig at the Whittle Laboratory, University of Cambridge. It is connected to an open-circuit suction wind tunnel and is designed for taking both the aerodynamic loss and the heat transfer measurements of different hole geometries. The design is similar to the low-speed experimental facility used by Sargison *et al.* [13, 14]. The mainstream flow is taken directly from atmosphere before entering a contraction and a flow conditioning (honeycomb) section. The Perspex test section has a square cross-section of 252 $mm \times 252$ mm. The bottom wall of the test section is the flat plate, which has a thickness of 17.5 mm. The plan view of the flat plate in Fig. 4 shows a cartridge with a row of 9 baseline cylindrical holes. The baseline cylindrical holes have a diameter of $D = 7$ mm, $\alpha = 35°$, $\beta = 0°$ and a hole pitch of $P/D = 3$. Different cooling hole geometries were drilled into cartridges and their details are given later. Subsequent references to the 'flat plate' experiments mean that the flat plate cartridge (no cooling holes) was used.

Underneath the cartridge is a plenum which supplies the coolant (Fig. 3). On a real blade, the coolant is supplied from an internal channel, which can have a large throughflow velocity. A plenum is used here to simplify the interpretation of the data, in particular the validation of the 3D Hartsel model. The coolant flow is taken from atmosphere and its pressure is increased with a 3 kW blower before entering the plenum. Between the blower and the plenum, is an International Standard ISO 5167 orifice plate [20,21] for coolant mass flowrate (m_c) measurement, which has an uncertainty of ± 1.2 % as calculated according to the approach stated in the International Standard. Inside the plenum, there is a gauze for conditioning the flow to be uniform.

The origin of the right handed xyz-axes of the rig is indicated in Figs. 3 and 4. The x-distance from the centre of the hole exit to the downstream end of the test section is 400 mm or 57.1 D.

Figure 3 also indicates the locations of stagnation pressure, static pressure and stagnation temperature measurements for both the mainstream inlet (label A) and the coolant plenum (label B). The inlet stagnation pressures were measured with Pitot tubes, while the corresponding static pressures were measured using static pressure tappings. The pressure measurements have an uncertainty of ± 0.5 % of $\frac{1}{2}\rho_g {V_g}^2$. The stagnation temperatures were measured with K-type thermocouples, which have an uncertainty of ± 0.35 K. The mainstream velocity, the mainstream density and the coolant density in the plenum were calculated from these inlet conditions. The coolant velocity in the cooling hole was calculated from the coolant mass flowrate and the cooling hole throat area. The coolant to mainstream density ratio, $DR = \rho_c/\rho_g$, is approximately 1.0 and the uncertainty in DR is ± 0.2 %. The amount of m_c can be adjusted to change the blowing ratio, $BR = (\rho_c V_c)/(\rho_g V_g)$; the velocity ratio, $VR = V_c/V_g$; and the momentum flux ratio, $IR = (\rho_c V_c^2)/(\rho_g V_g^2)$. The uncertainties in BR, VR and IR are ± 1.4 %, ± 1.4 % and ± 2.8 % respectively.

Aerodynamic loss measurements

The aerodynamic loss measurements were taken by area traverses of both a 5-hole probe and a 3-hole probe. The 5-hole probe head is a pyramid with a diameter of 2 mm and an included angle of 90°; the five pressure tappings are perpendicular to each face of the head (Dominy and Hodson [22]). The head of the 3-hole probe is a cobra probe, which consists of three tubes each with a diameter of 0.5 mm. The uncertainties of the flow yaw and pitch angles measured by the probes are estimated to be $\pm 0.2°$.

Figure 5 illustrates the measurement grid of the area traverse and also contours of stagnation pressure coefficient (C_{p0}) for the baseline cylindrical holes. C_{p0} is defined in Eqn. (7) and these contours are discussed in a later section. The traverse covers the area of 3 hole pitches in the lateral direction and $0.11 < z/D < 5.04$ in the wall normal direction. The 3-hole probe measures the region of $0.11 < z/D < 0.46$, with a grid size of 64 (lateral,

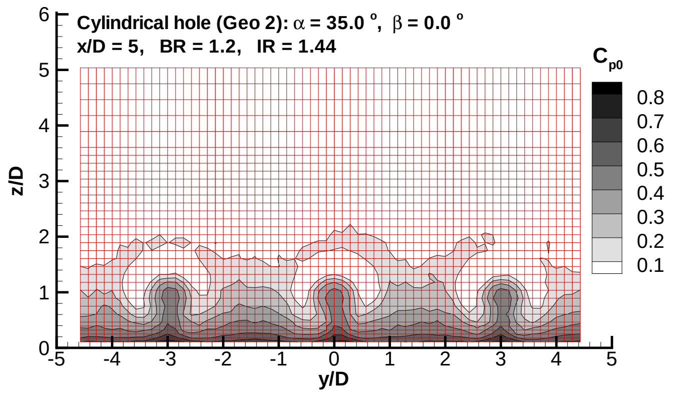

FIGURE 5: Measurement grid of the area traverse; contours of C_{p0} at the plane $x/D = 5$ for the baseline cylindrical holes

8 points across 1 D) × 6 (wall normal). The remaining region is measured by the 5-hole probe, with a grid size of 64 × 28. The results measured by the traverse correspond to the middle 3 holes of a cartridge (Fig. 4). Figure 5 shows that the interaction between the mainstream and the coolant is periodic across each hole pitch.

During the aerodynamic loss measurements, the heater mesh for heating the coolant (Fig. 3) is switched off. In addition, the uniform heat flux plate (Fig. 4) is replaced with a Perspex plate.

Calculating aerodynamic loss from experiments

The aerodynamic loss measured in the experiments is quantified in terms of $\zeta_{mix,KE}$, which is the experimental entropy loss coefficient for $\Delta\Sigma_{mix,KE}$. It is based on the entropy loss coefficient of Denton [23] and the control volume as shown in Fig. 6. The inlet 'g' is the mainstream plane at a distance upstream of the coolant ejection; the inlet 'c' is the coolant inlet; the mainstream and coolant mixture leaves the control volume at exit plane 'm', which is the mixed-out plane. The plane '2' is the plane where the area traverse measurements are taken. The measured data at the plane 2 are used to obtain the results at the mixed-out plane through control volume analysis. In the present study, the plane 2 is at $x/D = 5$. The intentions of using the mixed-out plane as the exit plane are: firstly, to remove the influence of the location of plane 2 on aerodynamic loss; secondly, to enable a consistent comparison of aerodynamic loss of different cooling hole geometries.

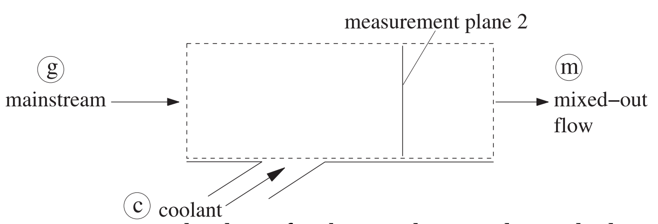

FIGURE 6: Control volume for the aerodynamic loss calculation

$\zeta_{mix,KE}$ can be calculated from the following stagnation pressure coefficients,

$$\zeta_{mix,KE} \approx -\phi \left[\frac{p_{01g} - p_{0c}}{p_{01g} - p_{1g}}\right] + (1+\phi)\left[\frac{p_{01g} - p_{0m,cool}}{p_{01g} - p_{1g}}\right] - \left[\frac{p_{01g} - p_{0m,BL}}{p_{01g} - p_{1g}}\right] \tag{3}$$

where $\phi = m_c/m_g$ and m_g is based on the total traverse area of the 5-hole probe and the 3-hole probe, subscript '1g' represents the mainstream conditions as measured at the rig inlet, subscript 'm,BL' represents the mixed-out flow obtained from a boundary layer flow with no coolant ejection (flate plate experiment) and subscript 'm,cool' means the mixed-out flow obtained when there is coolant ejection. The derivation of Eqn. (3) is shown in Appendix A.

Following the approaches by Friedrichs [24], Day *et al.* [8] and Sargison *et al.* [13, 14], the measured aerodynamic loss can be split into two components: (i) aerodynamic loss due to the mixing of the mainstream and the coolant (aerodynamic mixing loss); (ii) aerodynamic loss generated inside the cooling hole. This is done by using two definitions of p_{0c}. For the first definition, $p_{0c,def1}$ is the measured coolant stagnation pressure in the plenum. For the second definition, $p_{0c,def2}$ is the coolant stagnation pressure at the hole exit. The exact $p_{0c,def2}$ cannot be obtained since no data across the cooling hole exit are available in the present study. Nonetheless, a pragmatic approach is to estimate $p_{0c,def2}$ with the following equation.

$$p_{0c,def2} \approx \overline{p_2} + \frac{1}{2}\rho_c V_c^2 \tag{4}$$

$p_{0c,def2}$ is estimated with the following assumptions: (i) the coolant flow is one-dimensional; (ii) the static pressure at the cooling hole exit is equal to the area-averaged static pressure measured at the plane 2 ($\overline{p_2}$); (iii) the coolant velocity (V_c) is in the direction set by α and β, such that V_c can be calculated from the coolant mass flowrate and the hole throat area.

Denoting the loss coefficients obtained by the two p_{0c} definitions as $\zeta^{def1}_{mix,KE}$ and $\zeta^{def2}_{mix,KE}$, we can obtain:

1. $\zeta_{total} = \zeta^{def1}_{mix,KE}$ = $\zeta_{mix} + \zeta_{hole}$
2. $\zeta_{mix} = \zeta^{def2}_{mix,KE}$ = aerodynamic mixing loss
3. $\zeta_{hole} = \zeta^{def1}_{mix,KE} - \zeta^{def2}_{mix,KE}$ = aerodynamic loss inside the hole

The authors acknowledge that the choice of $p_{0c,def2}$ is somewhat arbitrary. Hence, the split between ζ_{mix} and ζ_{hole} (but not ζ_{total}) is uncertain.

The uncertainty in ζ^{total} was estimated to be ±0.002. In addition, the repeatability of the aerodynamic loss experiments has been assessed. This was done by measuring ζ^{total} of the baseline cylindrical hole at three flow conditions of $IR = 0.16$, 0.64 and 1.44. At each flow condition, three repeated measurements were taken. The results are presented in Fig. 7. At every IR, the

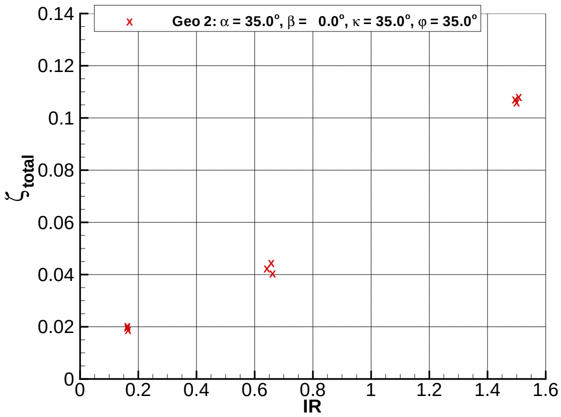

FIGURE 7: ζ^{total} against IR for the baseline cylindrical hole (Geo 2)

data for ζ_{total} were close. The biggest spread in the data is at $IR = 0.64$, with a magnitude of 0.004.

Heat transfer measurements

The convective heat flux to the blade surface when there is film cooling can be quantified by measuring the heat transfer coefficient in the presence of film cooling (h_f) and the adiabatic film cooling effectiveness (η) (Goldstein [25]). A useful film cooling heat transfer performance parameter is the net heat flux reduction (*NHFR*) by Sen *et al.* [26]. It is the ratio of reduction of the heat transfer with film cooling to the heat transfer without film cooling, which is defined as

$$NHFR = 1 - \frac{h_f}{h_{nfc}}(1 - \eta\theta) \tag{5}$$

where h_{nfc} is the heat transfer coefficient with no film cooling. θ is a non-dimensional temperature defined as

$$\theta = \frac{T_{01g} - T_{0c}}{T_{01g} - T_w} \tag{6}$$

where T_w is the wall temperature. θ is taken to be $\theta = 1.46$ in the present study, which is representative of real engine conditions (Sargison [13]). *NHFR* combines both η and h_f into a single parameter, which shows the net benefit of film cooling.

It is not within the scope of the present paper to report the heat transfer measurements setup and method in detail. The technique implemented is the liquid crystal thermography with a steady-state heat transfer, similar to that used by Sargison *et al.* [13, 14]. Under this technique, a narrow-band thermochromic liquid crystal (TLC) is used. The uniform heat flux plate, which supplies heat flux into the flow, is also installed in the test section (Fig. 4). In addition, the heater mesh as shown in Fig. 3 is switched on to increase the coolant temperature. The increase in coolant temperature is such that $DR \approx 1.0$. η, h_f and *NHFR* can be obtained through this technique. The experimental setup has been validated by comparing η and h_f results of the baseline cylindrical hole with the data by Sargison [13], Goldstein *et al.* [27], Schmidt *et al.* [28], Sen *et al.* [26] and Baldauf *et al.* [29, 30].

Film cooling hole geometries

The cooling hole geometries which have been tested comprised of two groups. The first group consists of eight cylindrical holes with different values of α and β. Table 1 summarises α, β, κ, L/D and φ of these holes. Geo 2 is the baseline cylindrical hole. Both Geo 2 and Geo 7 are illustrated in Fig. 8. From Eqn. (2), Geo 2, Geo 7, Geo 8 and Geo 9 form a set of cylindrical holes with $\kappa = 35°$; while Geo 10, Geo 11, Geo 12 and Geo 13 form another set of cylindrical holes with $\kappa = 60°$.

TABLE 1: Parameters of two sets of cylindrical holes

Geometry	α (°)	β (°)	κ (°)	L/D	φ (°)
Geo 2	35.0	0.0	35.0	4.4	35.0
Geo 7	20.0	29.3	35.0	8.4	17.3
Geo 8	25.0	25.3	35.0	6.5	22.5
Geo 9	30.0	18.9	35.0	5.3	28.2
Geo 10	60.0	0.0	60.0	2.9	60.0
Geo 11	30.0	54.7	60.0	8.7	16.8
Geo 12	35.0	52.4	60.0	7.1	20.5
Geo 13	55.0	29.3	60.0	3.5	45.6

The second group consists of five streamwise holes ($\alpha = 35.0°$, $\beta = 0.0°$) with different hole inlet and hole exit geometries. They are: baseline cylindrical hole (Geo 2), trenched hole, fan-shaped hole (known here as Fan), drilled fan-shaped hole (D-Fan) and smooth drilled fan-shaped hole (SD-Fan). Figure 8 shows the drawings of these geometries.

The trenched hole is similar to Configuration 7 of Dorrington *et al.* [17]. It has a cylindrical hole inlet of diameter $1\ D = 7\ mm$ and $L/D = 3.1$. The hole exit is embedded in a trench with a depth of $0.75\ D$, which spans laterally across the entire row of holes. The perpendicular upstream wall of the trench is at the hole exit leading edge, while the perpendicular downstream wall is at the hole exit trailing edge. This trenched hole configuration has a good adiabatic film cooling effectiveness performance (Dorrington *et al.* [17] and Waye and Bogard [31]).

The Fan has a cylindrical hole inlet of diameter $1\ D = 7\ mm$ and $L/D = 1.9$. Beyond the throat, there is a lateral expansion with an expansion angle of $e = 17.5°$. This is the angle between axes F1 and C or axes F2 and C, measured on plane E where these axes lie. Plane E is inclined at an angle of $\alpha = 35.0°$.

The D-Fan and the SD-Fan are similar to the Fan. However, the D-Fan and the SD-Fan have hole inlets and hole exits which are laterally expanded. The D-Fan was created by drilling along

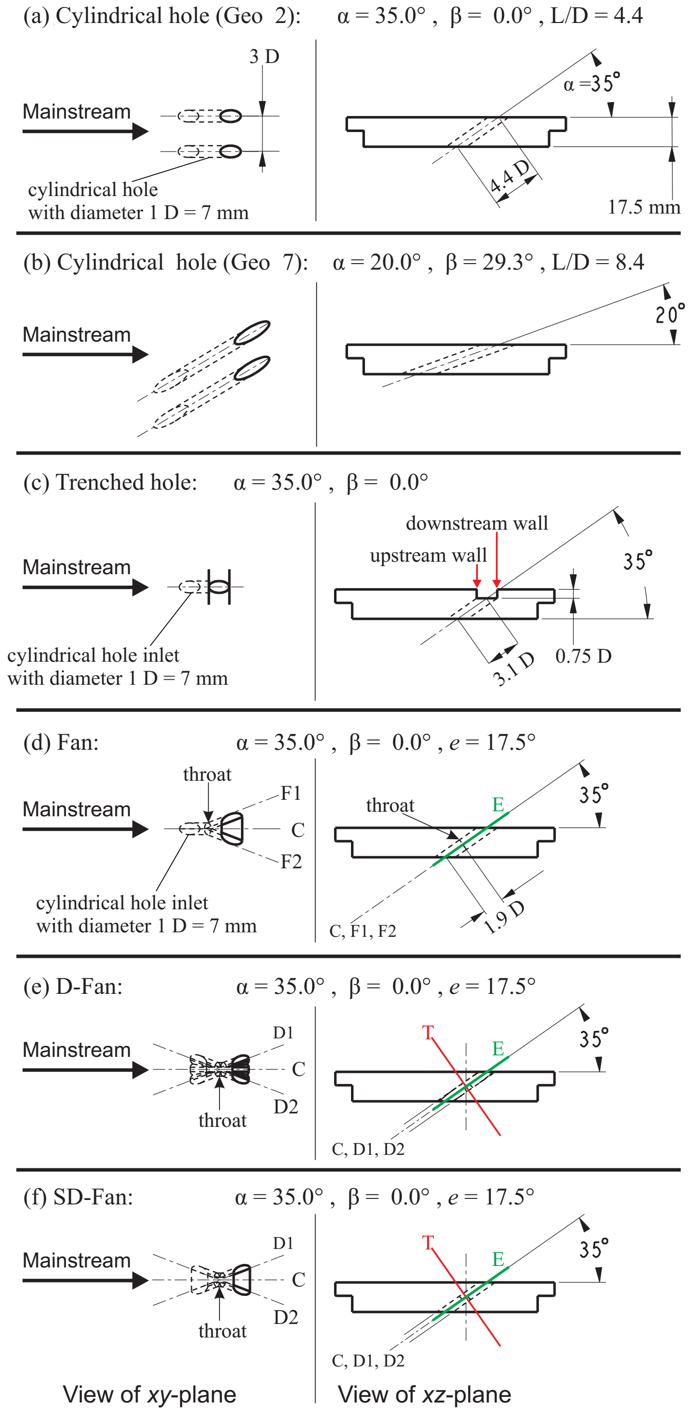

FIGURE 8: Drawings of the cylindrical holes (Geo 2, Geo 7), the trenched hole, the Fan, the D-Fan and the SD-Fan

axes C, D1 and D2 (Fig. 8). Axes D1 and C or axes D2 and C form a lateral expansion angle of $e = 17.5°$ at the hole inlet and at the hole exit. The throat lies on Plane T. The throat cross-sectional area is the same as that of the cylindrical hole.

The SD-Fan was created in the same way as the D-Fan. However, there was an extra manufacturing step to remove the sharp corners or cusps inside the D-Fan, created by drilling along axes C, D1 and D2. Hence, the SD-Fan has smooth hole inlet and hole exit. Nonetheless, this makes the SD-Fan more expensive to manufacture than the D-Fan. The SD-Fan also has $e = 17.5°$. The Fan is used as a reference geometry for the D-Fan and the SD-Fan, since all three geometries have the same e.

For each cooling hole geometry in the present study, a row of 9 holes with a hole pitch of $P/D = 3$ was machined into a separate cartridge (Fig. 4). The surface of the present experiments has (*average roughness*)/(*hole diameter*) ≈ 0.0014. This value is 0.0025 for a real airfoil which has been newly manufactured, polished and first put into service (nominal surface roughness = 2.5 μm, nominal hole diameter = 1 mm, Bunker [19]).

Experimental flow conditions

The rig was run at a nominal mainstream velocity of 25 $m\,s^{-1}$. The Reynolds number (Re_D) based on the mainstream velocity and the cylindrical hole diameter is 11,500, which is an engine representative value. At the plane $x/D = -2.5$, the inlet boundary layer properties are: boundary layer thickness, $\delta/D = 1.95$; displacement thickness, $\delta^*/D = 0.33$; momentum thickness, $\theta_{BL}/D = 0.23$; and shape factor, $H = 1.44$. The rig freestream turbulence intensity is $Tu = 0.5$ %.

As stated earlier, $DR \approx 1.0$ in the present study, while an engine representative DR is 2. Nevertheless, Day *et al.* [8] have shown that IR is a suitable scaling parameter for film cooling studies with varying coolant densities. In addition, Thole *et al.* [32], Day *et al.* [8], and Walters and Leylek [33] found that amongst the flow ratios (BR, VR and IR), the best scaling parameter for the thermal field, flow structures and aerodynamic loss is IR . For each hole geometry in the present study, measurements were taken at three flow conditions:

1. $IR = 0.16$ ($BR = 0.4$, $VR = 0.4$)
2. $IR = 0.64$ ($BR = 0.8$, $VR = 0.8$)
3. $IR = 1.44$ ($BR = 1.2$, $VR = 1.2$)

These flow conditions were chosen so that the coolant ejection through the baseline cylindrical hole (Geo 2) corresponds to the three flow scenarios categorised by Thole *et al.* [32]. These scenarios are: (i) $IR < 0.4$, the coolant is fully attached to the surface downstream of the hole exit; (ii) $0.4 < IR < 0.8$, the coolant is detached from the surface and then reattaches to the surface; (iii) $IR > 0.8$, the coolant is fully detached from the surface.

RESULTS FOR CYLINDRICAL HOLES WITH DIFFERENT α AND β BUT WITH THE SAME κ

Flow structures

A brief overview of the flow structures is given here, which helps to explain subsequent discussion of the aerodynamic loss

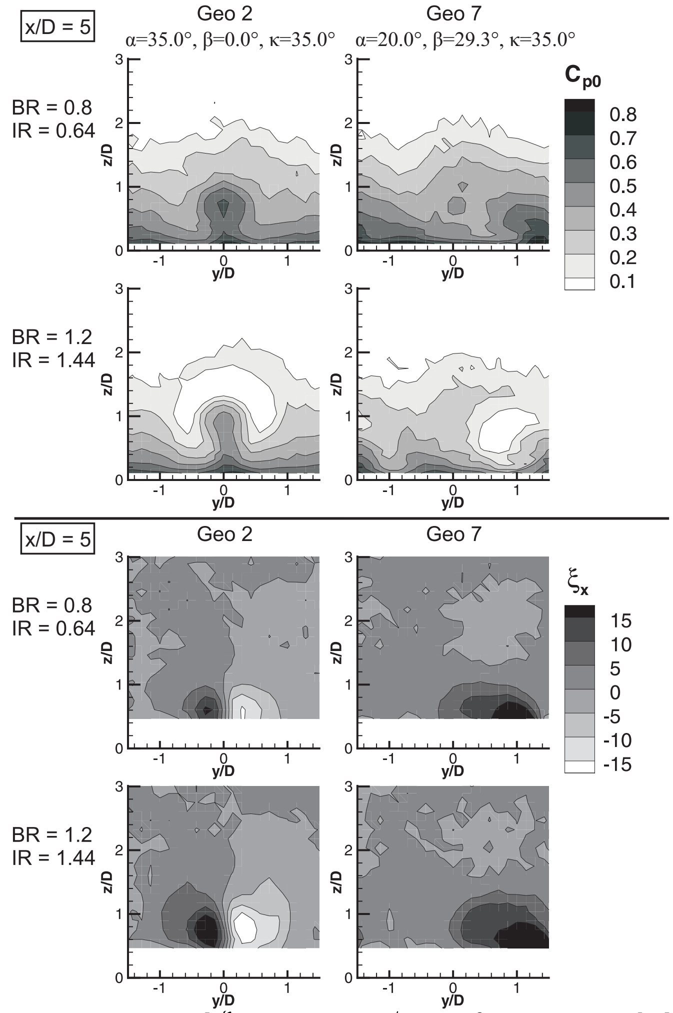

FIGURE 9: C_{p0} and ξ_x contours at $x/D = 5$ for streamwise hole (Geo 2) and compound angle hole (Geo 7); $IR = 0.64$ and 1.44

results. Figure 9 shows contours of stagnation pressure coefficient (C_{p0}) and streamwise component of vorticity (ξ_x) at the plane $x/D = 5$, for the streamwise hole (Geo 2) and the compound angle hole (Geo 7) at $IR = 0.64$ and 1.44. C_{p0} is defined as

$$C_{p0} = \frac{p_{01g} - p_0}{p_{01g} - p_{1g}} \tag{7}$$

where p_0 is the local stagnation pressure. ξ_x is positive in the anticlockwise direction; the ξ_x contours are only shown from $z/D > 0.46$, since that is the region of the 5-hole probe traverse.

According to Leylek and Zerkle [34], as the coolant flows from the plenum into the cooling hole, the flow turns around the sharp corner on the downstream side of the hole inlet and separates. A pair of counter-rotating vortices is also formed inside the hole. When the vortices leave the hole exit, for the streamwise hole (Geo 2), the vortices entrain the hot mainstream and form a pair of kidney-shaped vortices (Fric and Roshko [35]). These are observed in the ξ_x contours for Geo 2. The kidney vortices lift the coolant away from the wall, as illustrated by the C_{p0} contours which show a symmetrical coolant core above the wall. As IR is increased from 0.64 to 1.44, the kidney vortices become stronger and move further away from the wall.

For the compound angle holes (Geo 7, Geo 8 and Geo 9), McGovern and Leylek [10], and Lee *et al.* [9] found that the counter-rotating vortices which originate from the hole become asymmetric and a single dominant vortex forms. This dominant vortex can be seen in the ξ_x contours for Geo 7 in Fig. 9. The vortex increases the coolant lateral spreading. The C_{p0} contours for Geo 7 show that the coolant core is translated laterally toward the positive y-direction. As IR is increased, the dominant positive vortex becomes stronger.

Aerodynamic loss: cylindrical holes with $\kappa = 35.0°$

Figure 10 shows the variations of the aerodynamic mixing loss (ζ_{mix}) with IR. As IR is increased, ζ_{mix} rises due to the increase in the coolant mass flowrate (m_c). For the streamwise hole, the kidney vortices become stronger and the coolant is lifted further away from the wall; for the compound angle holes, the dominant vortex also becomes stronger. As a result, there is more mixing of the mainstream and the coolant, which leads to a higher loss. ζ_{mix} predicted by the 3D Hartsel model at $\kappa = 35.0°$ is also plotted on Fig. 10. The results for all four geometries at $IR = 0.16$, 0.64 and 1.44 are close to the 3D Hartsel model prediction at $\kappa = 35.0°$. The maximum absolute difference between the experimental results and the prediction is 0.008.

All the geometries have an *estimated* $\kappa = 35.0°$, where the coolant ejection direction is assumed to follow the geometry angles α and β, Eqn. (2). However, in a real flow, the *effective* flow exit angle could deviate from these angles, as shown by the CFD simulation of Hyams and Leylek [36]. They assessed cylindrical holes with $\alpha = 35.0°$, $\beta = 0.0°$ and $L/D = 4$; IR of the simulation is 0.975. They found that at the hole exit, the *effective* inclination angle of the flow is in the range of 31.0° to 33.0°. Based on this, the 3D Hartsel model prediction at $\kappa = 31.0°$ is also plotted on Fig. 10. ζ_{mix} of all the geometries is close to both the 3D Hartsel model at $\kappa = 35.0°$ and $\kappa = 31.0°$. This suggests that the *effective* κ of the geometries lie between 31.0° and 35.0°.

Figure 11 shows the variations of the aerodynamic loss generated inside the cooling hole (ζ_{hole}) with IR. This loss is mainly associated with the coolant separation at the sharp hole inlet. At $IR = 0.16$, the results are the same for all the geometries. At $IR = 0.64$, there is a small spread of 0.008. However, at $IR = 1.44$, the spread is 0.02 and ζ_{hole} increases in the following order: Geo 2, Geo 9, Geo 8 and Geo 7. According to McGovern and Leylek [10], the flow around the hole inlet and throughout the majority of the hole is sensitive to angle φ. This flow is less sensitive to changes at the hole exit due to the change in β. The detrimental coolant separation at the hole inlet becomes stronger

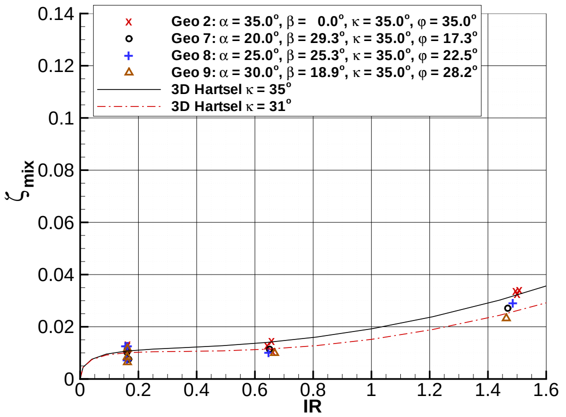

FIGURE 10: ζ_{mix} against IR for cylindrical holes with $\kappa = 35^\circ$

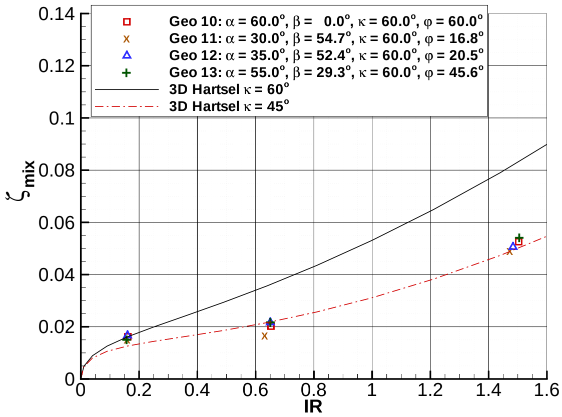

FIGURE 12: ζ_{mix} against IR for cylindrical holes with $\kappa = 60^\circ$

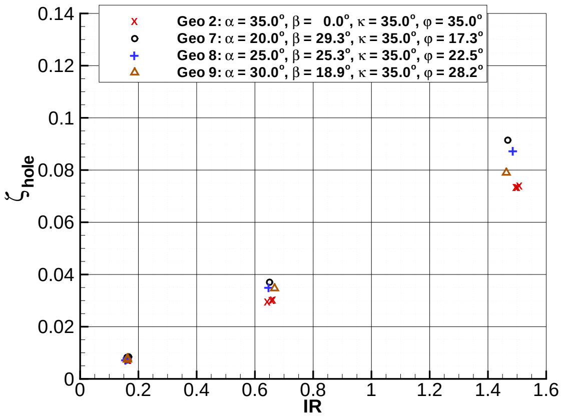

FIGURE 11: ζ_{hole} against IR for cylindrical holes with $\kappa = 35^\circ$

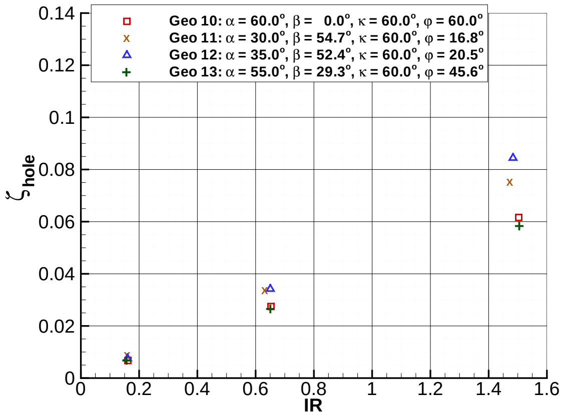

FIGURE 13: ζ_{hole} against IR for cylindrical holes with $\kappa = 60^\circ$

as angle φ decreases and as IR increases. φ of the geometries in decreasing order is also Geo 2, Geo 9, Geo 8 and Geo 7. This may explain the spread in the results.

Aerodynamic loss: cylindrical holes with $\kappa = 60.0^\circ$

Figure 12 shows the variations of ζ_{mix} with IR for the $\kappa = 60.0^\circ$ set. The results for all four geometries at $IR = 0.16$, 0.64 and 1.44 are close to each other, with a maximum spread of 0.005. In other words, their aerodynamic mixing loss due to the mixing of the mainstream and the coolant is in close agreement, despite differences in α and β. This is an important finding. α of these geometries are from 30.0° to 60.0° and β spans from 0.0° to 54.7° (Table 1). ζ_{mix} increases with IR, for the same reasons as stated for the $\kappa = 35.0^\circ$ set.

When ζ_{mix} of the geometries is compared to the prediction by the 3D Hartsel model with $\kappa = 60.0^\circ$, the results only match at $IR = 0.16$. At $IR = 0.64$ and 1.44, the 3D Hartsel model over-predicts the loss. In Fig. 12, the loss prediction by the 3D Hartsel model with $\kappa = 45.0^\circ$ is also plotted; it compares well with ζ_{mix} for all the geometries at $IR = 0.16$, 0.64 and 1.44. This suggests that the *effective* κ of these geometries is $\approx 45.0^\circ$.

The results for ζ_{hole} are presented in Fig. 13. This loss increases with IR. ζ_{hole} is the same for all the geometries at $IR = 0.16$. At $IR = 0.64$, ζ_{hole} is the same for Geo 11 and Geo 12; ζ_{hole} is also the same for Geo 10 and Geo 13. This can be explained by the φ values. φ of Geo 11 and Geo 12 are 16.8° and 20.5° respectively; φ for Geo 10 and Geo 13 are 60.0° and 45.6° respectively. At $IR = 1.44$, ζ_{hole} for all four geometries is different, which increases in the following order: Geo 13, Geo 10, Geo 11 and Geo 12. The reasons for this spread are not known.

TABLE 2: $\zeta_{hole}/\zeta_{total}$ in % for the $\kappa = 35^\circ$ and $\kappa = 60^\circ$ sets of cylindrical holes; $IR = 0.16$, 0.64 and 1.44

	$IR = 0.16$	$IR = 0.64$	$IR = 1.44$
Holes with $\kappa = 35^\circ$	43 %	76 %	75 %
Holes with $\kappa = 60^\circ$	32 %	60 %	57 %

Table 2 shows the loss generated inside the cooling hole (ζ_{hole}) as a percentage of the total loss (ζ_{total}) for the $\kappa = 35.0^\circ$ set and $\kappa = 60.0^\circ$ set of cylindrical holes at $IR = 0.16$, 0.64 and 1.44. The results are calculated by averaging the data for all four geometries of the same set. It is interesting to note that at $IR = 0.64$ and 1.44, more than 57 % of the total loss is generated inside the holes. Hence, it is worthwhile finding ways to reduce ζ_{hole}, such as by modifying the hole inlet geometry. The influence of different hole inlet geometries on ζ_{hole} is investigated in a later section of this paper.

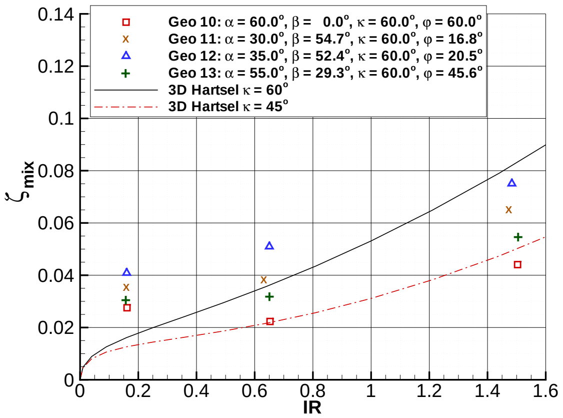

FIGURE 14: ζ_{mix} against IR for cylindrical holes with $\kappa = 60°$; calculated with a uniform mixed-out profile

The flow at the mixed-out plane is required to calculate the aerodynamic loss results. The mixed-out flow is not obtained by mixing-out in both the y-direction and the z-direction, which would produce a uniform mixed-out profile. Instead, the mixed-out flow in the present study (e.g. Fig. 12) is calculated by mixing-out in the lateral y-direction only, as this was felt to be more representative of the mixing process in film cooling application. The choice of the mixed-out approach can be clarified by comparing Fig. 14 with Fig. 12. Both figures are for the same geometries, however ζ_{mix} in Fig. 14 is calculated from a uniform mixed-out profile. Contrary to Fig. 12, ζ_{mix} in Fig. 14 for all the geometries is no longer in agreement at $IR = 0.16$, 0.64 and 1.44.

Heat transfer results

The heat transfer performance of cylindrical holes with the same aerodynamic mixing loss (same κ) is compared by assessing their spatially averaged net heat flux reduction ($\overline{\overline{NHFR}}$) at $IR = 0.16$, 0.64 and 1.44. $\overline{\overline{NHFR}}$ is calculated by averaging $NHFR$ results on the wall across the region of $7 < x/D < 45$ and $-4.5 < y/D < +4.5$ (lateral, 3 hole pitches). Results are not available for $x/D < 7$, due to the location of the uniform heat flux plate leading edge which is at $x/D = 5.7$ (Fig. 4). This shortcoming must be taken into account in the analysis of $\overline{\overline{NHFR}}$, since $\overline{\overline{NHFR}}$ is dependent on the region over which the averaging takes place. $\overline{\overline{NHFR}}$ therefore indicates the relative heat transfer performance of the geometries.

The results for the $\kappa = 35.0°$ set of cylindrical holes are presented in Fig. 15. All the geometries have different heat transfer performance. The compound angle holes (Geo 7, Geo 8 and Geo 9) have higher $\overline{\overline{NHFR}}$ than the streamwise hole (Geo

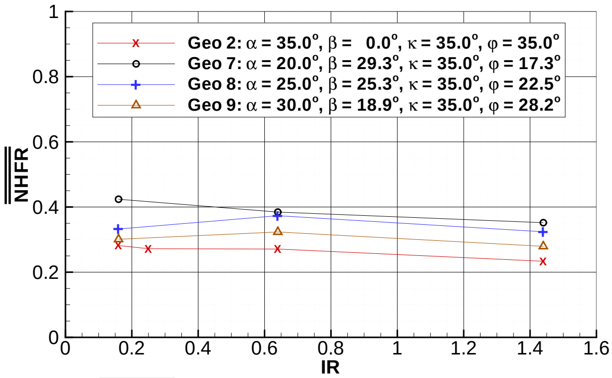

FIGURE 15: $\overline{\overline{NHFR}}$ against IR; cylindrical holes with $\kappa = 35.0°$

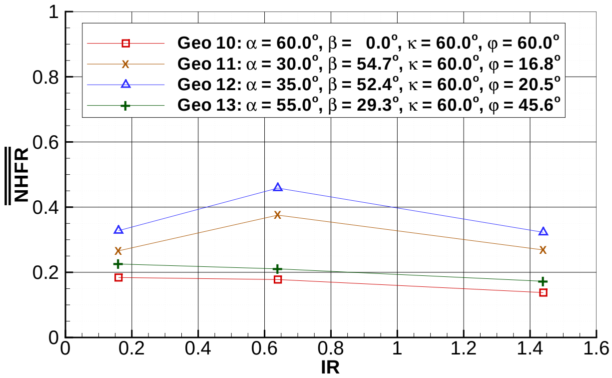

FIGURE 16: $\overline{\overline{NHFR}}$ against IR; cylindrical holes with $\kappa = 60.0°$

2). This is because the dominant vortex downstream of the compound angle hole exit helps to improve the coolant lateral spreading, and to reduce the coolant separation downstream of the hole exit. For Geo 2 and Geo 7, the decrease in $\overline{\overline{NHFR}}$ with increasing IR is associated with more coolant separation downstream of the hole exit. For Geo 8 and Geo 9, $\overline{\overline{NHFR}}$ increases from $IR = 0.16$ to 0.64 because the coolant coverage on the wall has improved; however $\overline{\overline{NHFR}}$ decreases when $IR = 1.44$ due to more coolant separation. Overall, Geo 7 has the best heat transfer performance, followed by Geo 8, Geo 9 and Geo 2. β of these geometries also decreases in the same order.

Figure 16 shows the corresponding heat transfer results for the $\kappa = 60.0°$ set of holes. Again, the four geometries have different heat transfer performance. The behaviour of $\overline{\overline{NHFR}}$ with IR is due to the same reasons as for the $\kappa = 35.0°$ set. Geo 12 has the best heat transfer performance, followed by Geo 11, Geo 13 and Geo 10. $\overline{\overline{NHFR}}$ results for the $\kappa = 35.0°$ set and the $\kappa = 60.0°$ set show that a large β is favourable for good heat transfer performance.

Comments on the cylindrical hole tests

The results for the $\kappa = 35.0°$ set and the $\kappa = 60.0°$ set confirm that, for the same flow conditions, the aerodynamic mixing loss ($\Delta\Sigma_{mix,KE}$) is the same for cylindrical cooling holes with different α and β but with the same κ. The angle κ combines α and β into a single parameter. A low κ is desired in order to minimise the aerodynamic mixing loss. However, for the best heat transfer performance, a large β is preferred.

RESULTS FOR FIVE DIFFERENT HOLE GEOMETRIES ($\alpha = 35.0°$, $\beta = 0.0°$)

Aerodynamic loss

ζ_{mix} for all the geometries increases with IR as shown in Fig. 17. The analysis of ζ_{mix} for the cylindrical hole (Geo 2) has been discussed previously. Overall, ζ_{mix} is the highest for the trenched hole. There are sharp edges at the trench upstream and downstream walls, which can lead to flow separation and so contribute toward the high loss of the trenched hole.

ζ_{mix} of the D-Fan and the SD-Fan is the same at all three momentum flux ratios. Referring to the results for all five geometries at $IR = 1.44$, ζ_{mix} for the Fan, the D-Fan and the SD-Fan are close to each other with a spread of 0.006, while their ζ_{mix} are ≈ 0.02 higher than that of the cylindrical hole and ≈ 0.02 lower than that of the trenched hole. From Fig. 8, the Fan, the D-Fan and the SD-Fan have laterally expanded hole exits with $e = 17.5°$; however the hole inlet of the Fan is cylindrical, while the hole inlets of the D-Fan and the SD-Fan are laterally expanded. Despite the Fan, the D-Fan and the SD-Fan having different hole inlets, their results at $IR = 1.44$ suggest that the cooling hole exit geometry has a stronger influence on ζ_{mix} than the cooling hole inlet geometry.

ζ_{mix} prediction from the 3D Hartsel model at $\kappa = 35.0°$ is also plotted on Fig. 17. ζ_{mix} for the cylindrical hole matches the 3D Hartsel model at all three momentum flux ratios.

The results for ζ_{hole} are presented in Fig 18. At $IR = 0.16$, the loss for all the geometries is close to each other, with a spread of 0.004. At $IR = 0.64$ and 1.44, the cylindrical hole has the highest ζ_{hole}, which increases with IR. This is due to the detrimental coolant separation at the hole inlet.

ζ_{hole} for the trenched hole and the Fan is the same, which increases with IR. Both geometries have the same cylindrical hole inlets, with $L/D = 3.1$ for the trenched hole and $L/D = 1.9$ for the Fan. However, their hole exit geometries are different. This suggests that the loss generated inside the cooling hole is dominated by the hole inlet geometry.

The D-Fan and the SD-Fan have the same ζ_{hole}, which remains approximately constant as IR is increased. Their ζ_{hole} is also the lowest of all the geometries. Such favourable performance is likely due to the laterally expanded hole inlets of both geometries. Their inlets reduce the turning of the coolant as it moves from the plenum into the holes. As a result, there should be less coolant separation when compared to a cylindrical hole inlet. Furthermore, the hole inlets of the D-Fan and the SD-Fan are convergent which accelerates the flow. The console also has

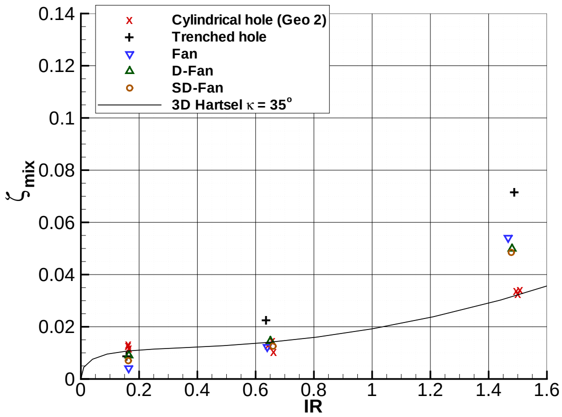

FIGURE 17: ζ_{mix} against IR for different geometries; $\alpha = 35.0°$ and $\beta = 0.0°$

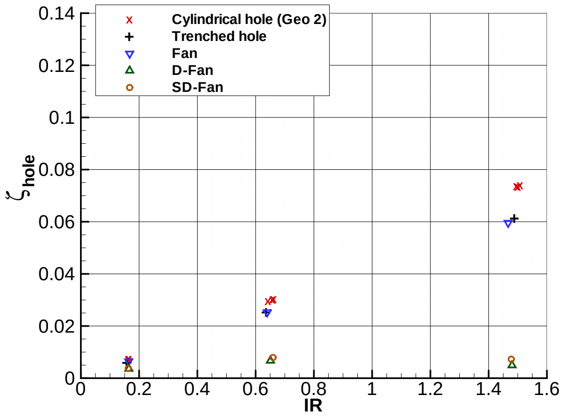

FIGURE 18: ζ_{hole} against IR for different geometries; $\alpha = 35.0°$ and $\beta = 0.0°$

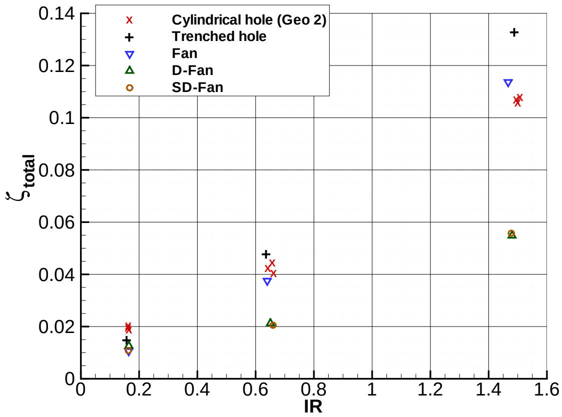

FIGURE 19: ζ_{total} against IR for different geometries; $\alpha = 35.0°$ and $\beta = 0.0°$

a convergent geometry and Sargison *et al.* [14] attributed the low aerodynamic loss of the console to this flow acceleration. They reasoned that the acceleration reduces the turbulence within the cooling hole and hence lowers the aerodynamic loss.

By comparing ζ_{total} for all the geometries in Fig. 19, there is a small spread in the data of 0.01 at $IR = 0.16$, which increases to 0.08 at $IR = 1.44$. The highest ζ_{total} is generated by the cylindrical hole at $IR = 0.16$ and by the trenched hole at $IR = 0.64$ and 1.44. The D-Fan and the SD-Fan have the same ζ_{total}, which is also the lowest of all the geometries at $IR = 0.16$, 0.64 and 1.44. ζ_{total} (D-Fan, SD-Fan) is 56 % and 49 % of ζ_{total} (Fan) at $IR = 0.64$ and 1.44 respectively. This is due to the low ζ_{hole} for the D-Fan and the SD-Fan.

Table 3 shows $\zeta_{hole}/\zeta_{total}$ in % for the geometries. The results at $IR = 0.16$ are not presented, as the magnitudes of ζ_{total} for the geometries are relatively small. Out of the total loss, ≈ 70 % and ≈ 50 % is generated inside the cylindrical hole and the trenched hole respectively. For the Fan, at least 52 % of the total loss is generated inside the hole. On the other hand, a maximum of 39 % of the total loss is generated inside the D-Fan and the SD-Fan. Thus, the loss generated inside the cylindrical hole, the trenched hole and the Fan can potentially be reduced significantly by using a laterally expanded hole inlet, just like the D-Fan and the SD-Fan.

TABLE 3: $\zeta_{hole}/\zeta_{total}$ in % for different geometries; $IR = 0.64$ and 1.44

	$IR = 0.64$	$IR = 1.44$
Cylindrical hole	71 %	69 %
Trenched hole	53 %	46 %
Fan	67 %	52 %
D-Fan	32 %	9 %
SD-Fan	39 %	13 %

Heat transfer results

The variations of $\overline{\overline{NHFR}}$ with IR are illustrated in Fig. 20. The decrease in $\overline{\overline{NHFR}}$ is associated with coolant separation. For the cylindrical hole, $\overline{\overline{NHFR}}$ decreases gradually with IR. The $\overline{\overline{NHFR}}$ for the trenched hole increases by 0.11 when IR is increased from 0.16 to 0.36; however when IR is increased to 1.44, $\overline{\overline{NHFR}}$ decreases gradually by 0.05.

$\overline{\overline{NHFR}}$ for the Fan, the D-Fan and the SD-Fan at $IR = 0.16$ are close to each other, with a spread of 0.03. Their laterally expanded hole exits make their performance better than the cylindrical hole and the trenched hole. The lateral expansion diffuses the coolant, which improves the coolant lateral coverage and makes the coolant less susceptible to separation especially at higher IR. For the Fan, as IR is increased to 0.64, $\overline{\overline{NHFR}}$ increases by 0.24 and remains constant from $IR = 0.64$ to 1.44. For the D-Fan, $\overline{\overline{NHFR}}$ increases by 0.14 when IR is increased to 0.64; at $IR = 1.44$, $\overline{\overline{NHFR}}$ decreases to a level below that at $IR = 0.16$. Lastly, $\overline{\overline{NHFR}}$ for the SD-Fan only differs from $\overline{\overline{NHFR}}$ for the D-Fan by 0.03 at $IR = 0.64$; however at $IR = 1.44$, $\overline{\overline{NHFR}}$ for the SD-Fan decreases close to its value at $IR = 0.16$.

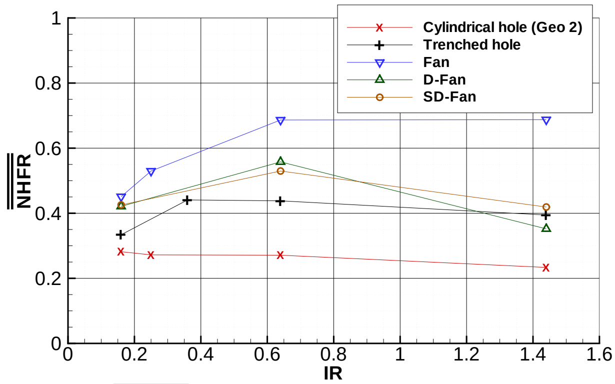

FIGURE 20: $\overline{\overline{NHFR}}$ against IR for different geometries; $\alpha = 35.0^\circ$ and $\beta = 0.0^\circ$

In general, the Fan has the best heat transfer performance (highest $\overline{\overline{NHFR}}$). This is followed by the D-Fan and the SD-Fan, then the trenched hole and finally the cylindrical hole.

Comments on the comparison of the five streamwise hole geometries

Amongst the five geometries, at $IR \leq 0.64$, the D-Fan and the SD-Fan are preferred. This is because they have the lowest aerodynamic loss and their heat transfer performance is good, which is between that of the Fan and the trenched hole. At $IR > 0.64$, the Fan is preferred due to its good heat transfer performance. However, there are penalties on the aerodynamic loss and the manufacturing cost.

Both the D-Fan and the SD-Fan have the same aerodynamic loss and their heat transfer performance is close to each other. Hence, these results imply that it is unnecessary to remove the sharp corners or cusps inside the D-Fan, in order to turn it into the SD-Fan (Fig. 8).

When the trenched hole and the D-Fan are compared, the trenched hole has a higher aerodynamic loss and a poorer heat transfer performance. However, no data are available to compare their manufacturing cost.

CONCLUSIONS

Experiments have been carried out on different film cooling hole geometries, in order to assess the influence of hole angles, hole inlet geometry and hole exit geometry on both the aerodynamic loss and the heat transfer performance. Two sets of cylindrical holes with different α and β but with the same κ of 35.0° and 60.0° respectively were tested. It was found that:

1. For the same flow conditions, cylindrical holes with different α and β but with the same κ have the same aerodynamic

mixing loss. However, the holes in the same κ set have different heat transfer performance, with the hole at the largest β being the best in this respect.

2. The experimental results support the use of κ to extend the 2D Hartsel model for the aerodynamic mixing loss to 3D, which has only been proven previously through analytical control volume analysis. Nonetheless, the 3D Hartsel model prediction based on κ is an overestimation, which is still reasonable and conservative for the design work. The model can be improved by using an *effective* κ. For the $\kappa = 35.0^\circ$ set of cylindrical holes, the results suggest that the *effective* κ is between 31.0° and 35.0°; for the $\kappa = 60.0^\circ$ set of cylindrical holes, it was found that the *effective* κ is $\approx 45.0^\circ$.

Measurements were also taken for five streamwise holes ($\alpha = 35.0^\circ$, $\beta = 0.0^\circ$) with different hole inlet and hole exit geometries: the cylindrical hole, the trenched hole, the fan-shaped hole (Fan), the D-Fan and the SD-Fan. The conclusions are:

3. At $IR = 0.64$ and 1.44, > 46 % of the total loss (ζ_{total}) is generated inside the cylindrical hole, the trenched hole and the Fan, due to the detrimental coolant separation at their cylindrical hole inlets. The loss generated inside these holes could be reduced by using a laterally expanded hole inlet, similar to those of the D-Fan and the SD-Fan. Such an inlet is convergent which accelerates the flow.
4. ζ_{total} (D-Fan, SD-Fan) is 56 % and 49 % of ζ_{total} (Fan) at $IR = 0.64$ and 1.44 respectively. This is due to the favourable laterally expanded hole inlets of the D-Fan and the SD-Fan.
5. In general, ζ_{total} is the highest for the trenched hole and the lowest for the D-Fan and the SD-Fan.
6. The heat transfer performance is the best for the Fan, followed by the D-Fan and the SD-Fan, then the trenched hole and finally the cylindrical hole.
7. The D-Fan and the SD-Fan have the same aerodynamic loss. Their heat transfer performance is close to each other. It is therefore unnecessary to turn the D-Fan into the SD-Fan.

Based on conclusions (1), (3) and (4), the guidelines for designers in choosing hole angles and hole geometries are: (i) minimise κ of cylindrical holes to obtain the lowest aerodynamic mixing loss; (ii) maximise β of cylindrical holes to achieve the best heat transfer performance; (iii) use a laterally expanded hole inlet to reduce the aerodynamic loss generated inside the hole.

ACKNOWLEDGEMENTS

The authors are grateful to Prof. John Denton for the discussions during the course of this study. The authors would like to thank Rolls-Royce plc. for funding this work and for the permission to publish this paper.

REFERENCES

[1] Rolls-Royce, 2005. *The Jet Engine*, 6th ed. Key Publishing Limited.

[2] Wilcock, R. C., Young, J. B., and Horlock, J. H., 2005. ‘‘The effect of turbine blade cooling on the cycle efficiency of gas turbine power cycles’’. *ASME J. Eng. Gas Turbines and Power*, ***127***, Jan, pp. 109--120.

[3] Young, J. B., and Wilcock, R. C., 2002. ‘‘Modeling the air-cooled gas turbine: Part 1 -- general thermodynamics’’. *ASME J. Turbomach.*, ***124***, Apr, pp. 207--213.

[4] Young, J. B., and Wilcock, R. C., 2002. ‘‘Modeling the air-cooled gas turbine: Part 2 -- coolant flows and losses’’. *ASME J. Turbomach.*, ***124***, Apr, pp. 214--222.

[5] Lim, C. H., Pullan, G., and Northall, J., 2010. ‘‘Estimating the loss associated with film cooling for a turbine stage’’. In Proceedings of ASME Turbo Expo 2010, Jun 14-18, Glasgow, UK, no. GT2010-22327.

[6] Hartsel, J. E., 1972. ‘‘Prediction of effects of mass-transfer cooling on the blade-row efficiency of turbine airfoils’’. In AIAA, 10th Aerospace Sciences Meeting, San Diego, Calif., USA, no. AIAA-72-11.

[7] Ito, S., Eckert, E. R. G., and Goldstein, R. J., 1980. ‘‘Aerodynamic loss in a gas turbine stage with film cooling’’. *Journal of Engineering for Power*, ***102***, Oct, pp. 964--970.

[8] Day, C. R. B., Oldfield, M. L. G., and Lock, G. D., 2000. ‘‘Aerodynamic performance of an annular cascade of film cooled nozzle guide vanes under engine representative conditions’’. *Experiments in Fluids*, ***29***, Aug, pp. 117--129.

[9] Lee, S. W., Kim, Y. B., and Lee, J. S., 1997. ‘‘Flow characteristics and aerodynamic losses of film-cooling jets with compound angle orientations’’. *ASME J. Turbomach.*, ***119***, Apr, pp. 310--319.

[10] McGovern, K. T., and Leylek, J. H., 2000. ‘‘A detailed analysis of film cooling physics: Part 2-- compound-angle injection with cylindrical holes’’. *ASME J. Turbomach.*, ***122***, Jan, pp. 113--221.

[11] Bunker, R. S., 2005. ‘‘A review of shaped hole turbine film-cooling technology’’. *Journal of Heat Transfer*, ***127***, Jul, pp. 441--453.

[12] Goldstein, R. J., Eckert, E. R. G., and Burggraf, F., 1974. ‘‘Effects of hole geometry and density on three-dimensional film cooling’’. *International Journal of Heat and Mass Transfer*, ***17***, pp. 595--607.

[13] Sargison, J. E., 2001. ‘‘Development of a novel film cooling hole geometry’’. PhD thesis, University of Oxford, Department of Engineering Science.

[14] Sargison, J. E., Guo, S. M., Oldfield, M. L., and Rawlinson, A., 2002. ‘‘A converging slot-hole film-cooling geometry - part 1: Low-speed flat-plate heat transfer and loss’’. *ASME J. Turbomach.*, ***124***, Jul, pp. 453--460.

[15] Porter, J. S., Sargison, J. E., Walker, G. J., and Henderson, A. D., 2007. ‘‘A comparative investigation of round and

fan-shaped cooling hole near flow fields''. In Proceedings of ASME Turbo Expo 2007, May 14-17, Montreal, Canada, no. GT2007-28185.
[16] Bunker, R. S., 2002. ''Film cooling effectiveness due to discrete holes within a transverse surface slot''. In IGTI Turbo Expo, Amsterdam, no. GT-2002-30178.
[17] Dorrington, J. R., Bogard, D. G., and Bunker, R. S., 2007. ''Film effectiveness performance for coolant holes embedded in various shallow trench and crater depressions''. In Proceedings of ASME Turbo Expo 2007, May 14-17, Montreal, Canada, no. GT2007-27992.
[18] Harrison, K. L., Dorrington, J. R., Dees, J. E., Bogard, D. G., and Bunker, R. S., 2009. ''Turbine airfoil net heat flux reduction with cylindrical holes embedded in a transverse trench''. *ASME J. Turbomach.*, ***131***, Jan, pp. 011012--1 to 011012--8.
[19] Bunker, R. S., 2008. ''The effects of manufacturing tolerances on gas turbine cooling''. In Proceedings of ASME Turbo Expo 2008, Jun 9-13, Berlin, Germany, no. GT2008-50124.
[20] International Standard, 2003. Measurement of fluid flow by means of pressure differential devices inserted in circular cross-section conduits runing full - part 1: General principles and requirements. ISO 5167-1.
[21] International Standard, 2003. Measurement of fluid flow by means of pressure differential devices inserted in circular cross-section conduits runing full - part 2: Orifice plates. ISO 5167-2.
[22] Dominy, R. G., and Hodson, H. P., 1992. ''An investigation of factors influencing the calibration of 5-hole probes for 3-D flow measurements''. In Proceedings of International Gas Turbine and Aeroengine Congress and Exposition Cologne, Germany June 1-4, no. 92-GT-216.
[23] Denton, J. D., 1993. ''Loss mechanisms in turbomachines''. *ASME J. Turbomach.*, ***115***, pp. 621--656.
[24] Friedrichs, S., 1997. ''Endwall film-cooling in axial flow turbines''. PhD thesis, Cambridge University Engineering Department, Whittle Laboratory.
[25] Goldstein, R. J., 1971. *Advances in Heat Transfer*, Vol. 7. New York, ch. Film Cooling, pp. 321--379.
[26] Sen, B., Schmidt, D. L., and Bogard, D. G., 1996. ''Film cooling with compound angle holes: Heat transfer''. *ASME J. Turbomach.*, ***118***, Oct, pp. 800--806.
[27] Goldstein, R. J., Jin, P., and Olson, R. L., 1999. ''Film cooling effectiveness and mass / heat transfer coefficient downstream of one row of discrete holes''. *ASME J. Turbomach.*, ***121***, Apr, pp. 225--232.
[28] Schmidt, D. L., Sen, B., and Bogard, D. G., 1996. ''Film cooling with compound angle holes: Adiabatic effectiveness''. *ASME J. Turbomach.*, ***118***, Oct, pp. 807--813.
[29] Baldauf, S., Scheurlen, M., Schulz, A., and Wittig, S., 2002. ''Correlation of film-cooling effectiveness from thermographic measurements at enginelike conditions''. *ASME J. Turbomach.*, ***124***, pp. 686--698.
[30] Baldauf, S., Scheurlen, M., Schulz, A., and Wittig, S., 2002. ''Heat flux reduction from film cooling and correlation of heat transfer coefficients from thermographic measurements at enginelike conditions''. *ASME J. Turbomach.*, ***124***, Oct, pp. 699--709.
[31] Waye, S., and Bogard, D., 2006. ''High resolution film cooling effectiveness measurements of axial holes embedded in a transverse trench with various trench configurations''. In Proceedings of ASME Turbo Expo 2006, May 8-11, 2006, Barcelona, Spain, no. GT2006-90226.
[32] Thole, K. A., Sinha, A. K., Bogard, D. G., and Crawford, M. E., 1992. Mean temperature measurements of jets with a crossflow for gas turbine film cooling application. Rotating Machinery Transport Phenomena, J. H. Kim and W. J. Yang, eds., Hemisphere Pub. Corp., New York.
[33] Walters, D. K., and Leylek, J. H., 2000. ''Impact of film-cooling jets on turbine aerodynamic losses''. *ASME J. Turbomach.*, ***122***, Jul, pp. 537--545.
[34] Leylek, J. H., and Zerkle, R. D., 1994. ''Discrete-jet film cooling: A comparison of computational results with experiments''. *ASME J. Turbomach.*, ***116***, Jul, pp. 358--368.
[35] Fric, T., and Roshko, A., 1994. ''Vortical structure in the wake of a transverse jet''. *J. Fluid Mech.*, ***279***, Nov, pp. 1--47.
[36] Hyams, D. G., and Leylek, J. H., 2000. ''A detailed analysis of film cooling physics: Part 3-- streamwise injection with shaped holes''. *ASME J. Turbomach.*, ***122***, Jan, pp. 122--132.

Appendix A: Derivation of the experimental entropy loss coefficient ($\zeta_{mix,KE}$)

The experimental entropy loss coefficient for $\Delta\Sigma_{mix,KE}$ ($\zeta_{mix,KE}$) is based on the entropy loss coefficient by Denton [23] and the control volume in Fig. 6. In this derivation, both mainstream and coolant are treated as the same perfect gases.

First, $\Delta\Sigma_{mix}$ is derived in terms of quantities which are measurable in experiments. By using the principle of superposition, the total rate of entropy creation due to irreversibilities generated in the control volume, $\Delta\Sigma_{total}$, is split into two components: (i)$\Delta\Sigma_{BL}$, entropy creation due to the boundary layer and (ii) $\Delta\Sigma_{mix}$, entropy creation due to the mixing of the mainstream and the coolant. Therefore,

$$\Delta\Sigma_{mix} = \Delta\Sigma_{total} - \Delta\Sigma_{BL} \tag{8}$$

$\Delta\Sigma_{BL}$ can be calculated by the same control volume in Fig. 6 but without the coolant ejection. This gives

$$\begin{aligned}\Delta\Sigma_{BL} &= m_g\left(s_{m,BL} - s_g\right)\\ &= m_g\left(c_p\, ln\frac{T_{0m,BL}}{T_{0g}} - R\, ln\frac{p_{0m,BL}}{p_{0g}}\right)\end{aligned} \tag{9}$$

where m_g is the mainstream mass flowrate based on the traverse area; s is the specific entropy; the subscripts have been defined in the main body of this paper. From the First Law, $T_{0m,BL} = T_{0g}$. Also, by using the series expansion of ln, Eqn. (9) reduces to

$$\begin{aligned}\Delta\Sigma_{BL} &= -m_g R\, ln \frac{p_{0m,BL}}{p_{0g}} \\ &\approx m_g R \left[\frac{p_{0g} - p_{0m,BL}}{p_{0m,BL}} \right] \end{aligned} \quad (10)$$

$\Delta\Sigma_{total}$ can be calculated in the same fashion, except that the control volume in Fig. 6 now includes the coolant ejection. The coolant is not heated and it is assumed that $T_{01g} = T_{0g} = T_{0c} = T_{0m}$. Therefore,

$$\begin{aligned}\Delta\Sigma_{total} &= m_g \left(s_{m,cool} - s_g \right) + m_c \left(s_{m,cool} - s_c \right) \\ &= -m_g R\, ln \frac{p_{0m,cool}}{p_{0g}} - m_c R\, ln \frac{p_{0m,cool}}{p_{0c}} \\ &\approx m_g R \left[\frac{p_{0g} - p_{0m,cool}}{p_{0m,cool}} \right] + m_c R \left[\frac{p_{0c} - p_{0m,cool}}{p_{0m,cool}} \right] \end{aligned} \quad (11)$$

Substituting Eqns. (10) and (11) into Eqn. (8), $\Delta\Sigma_{mix}$ becomes

$$\begin{aligned}\Delta\Sigma_{mix} \approx\ & m_g R \left[\frac{p_{0g} - p_{0m,cool}}{p_{0m,cool}} \right] + m_c R \left[\frac{p_{0c} - p_{0m,cool}}{p_{0m,cool}} \right] - \\ & m_g R \left[\frac{p_{0g} - p_{0m,BL}}{p_{0m,BL}} \right] \end{aligned} \quad (12)$$

$\Delta\Sigma_{mix}$ is made up of thermal mixing loss ($\Delta\Sigma_{mix,Q}$) and aerodynamic mixing loss ($\Delta\Sigma_{mix,KE}$). Since $T_{01g} = T_{0g} = T_{0c}$, there is no thermal mixing loss and $\Delta\Sigma_{mix} = \Delta\Sigma_{mix,KE}$.

The next step is to non-dimensionalise $\Delta\Sigma_{mix,KE}$ into $\zeta_{mix,KE}$, based on the definition by Denton [23].

$$\zeta_{mix,KE} = \left(\frac{T_{1g}}{m_g \frac{1}{2} V_{1g}^2} \right) \Delta\Sigma_{mix,KE} \quad (13)$$

The density is such that $\rho_{1g} = \rho_g = \rho_m$, using the ideal gas equation of state and noting that $T_0 \approx T$ for a low-speed flow,

$$\frac{R\, T_{1g}}{p_{om,BL}} \approx \frac{R\, T_{1g}}{p_{om,cool}} \approx \frac{1}{\rho_{1g}} \quad (14)$$

Using $\frac{1}{2}\rho_{1g}V_{1g}^2 = p_{01g} - p_{1g}$, $\phi = m_c/m_g$ and substituting Eqns. (12) and (14) into Eqn. (13), $\zeta_{mix,KE}$ becomes

$$\begin{aligned}\zeta_{mix,KE} \approx\ & \underbrace{\frac{1}{p_{01g} - p_{1g}} \left[p_{0g} + \phi\, p_{0c} - (1+\phi)\, p_{om,cool} \right]}_{A} - \\ & \underbrace{\frac{1}{p_{01g} - p_{1g}} \left[p_{0g} - p_{0m,BL} \right]}_{B} \end{aligned} \quad (15)$$

$$\zeta_{mix,KE} \approx \frac{1}{p_{01g} - p_{1g}} \left[\phi\, p_{0c} - (1+\phi)\, p_{om,cool} + p_{0m,BL} \right] \quad (16)$$

The term A in Eqn. (15) involves p_{0g}, p_{0c} and $p_{om,cool}$; this term is associated with the total entropy generation in the control volume in Fig. 6. The term B in Eqn. (15) which involves p_{0g} and $p_{om,BL}$ is associated with the entropy creation due to the boundary layer in the control volume. $\zeta_{mix,KE}$ in Eqn. (16) is independent of p_{0g} and the location of the plane where p_{0g} is measured.

Equation (16) can be written in terms of three different stagnation pressure coefficients,

$$\begin{aligned}\zeta_{mix,KE} \approx\ & -\phi \left[\frac{p_{01g} - p_{0c}}{p_{01g} - p_{1g}} \right] + (1+\phi) \left[\frac{p_{01g} - p_{0m,cool}}{p_{01g} - p_{1g}} \right] - \\ & \left[\frac{p_{01g} - p_{0m,BL}}{p_{01g} - p_{1g}} \right] \end{aligned} \quad (17)$$

which is the same as Eqn. (3) in the main body of this paper.